Environmental stresses induce karyotypic instability in colorectal cancer cells

Zhihao Tan[a,†,‡], Yong Jie Andrew Chan[a,†], Ying Jie Karen Chua[a], Samuel D. Rutledge[b], Norman Pavelka[c], Daniela Cimini[b], and Giulia Rancati[a,*]

[a]Institute of Medical Biology and [c]Singapore Immunology Network, Agency for Science, Technology and Research (A*STAR), Singapore 138648, Republic of Singapore; [b]Department of Biological Sciences and Biocomplexity Institute, Virginia Tech, Blacksburg, VA 24061

ABSTRACT **Understanding how cells acquire genetic mutations is a fundamental biological question with implications for many different areas of biomedical research, ranging from tumor evolution to drug resistance. While karyotypic heterogeneity is a hallmark of cancer cells, few mutations causing chromosome instability have been identified in cancer genomes, suggesting a nongenetic origin of this phenomenon. We found that in vitro exposure of karyotypically stable human colorectal cancer cell lines to environmental stress conditions triggered a wide variety of chromosomal changes and karyotypic heterogeneity. At the molecular level, hyperthermia induced polyploidization by perturbing centrosome function, preventing chromosome segregation, and attenuating the spindle assembly checkpoint. The combination of these effects resulted in mitotic exit without chromosome segregation. Finally, heat-induced tetraploid cells were on the average more resistant to chemotherapeutic agents. Our studies suggest that environmental perturbations promote karyotypic heterogeneity and could contribute to the emergence of drug resistance.**

Monitoring Editor
Rong Li
Johns Hopkins University

Received: Oct 11, 2018
Accepted: Oct 24, 2018

INTRODUCTION

Recent efforts in single-cell analysis of tumors revealed widespread genetic and nongenetic heterogeneity between cancer cells in spatially segregated areas of a given tumor mass (Gerlinger *et al.*, 2012), a phenomenon known as intratumor heterogeneity. Several studies correlated intratumor heterogeneity with drug resistance and poor prognosis (Swanton *et al.*, 2009; Danielsen *et al.*, 2016). Indeed, genetic and phenotypic variation between different clones in the same tumor pose challenges for patient stratification and treatment success. On one hand, characteristic signatures of disease progression might be distinct in different clones in the same tumor, hampering the design of tailored therapies (Burrell *et al.*, 2013). On the other hand, phenotypic variation could contribute to the emergence of drug resistance by acting as a substrate for selection and clonal expansion of resistant clones (Nowell, 1976). Therefore, understanding how eukaryotic cells acquire mutations is a fundamental question with important implications for reducing the emergence of chemotherapy resistance.

Cancer cell heterogeneity can come in the form of genetic, epigenetic, and karyotypic variation. Genetic heterogeneity has been widely recognized to contribute to tumorigenesis, and it has been linked to mutations in genes involved in DNA metabolism (Burrell *et al.*, 2013). Karyotypic variation, which encompasses whole-chromosome and ploidy changes, is pervasive in cancer cells (Gerlinger *et al.*, 2012) and has been recently listed as an "enabling characteristic" of tumorigenesis (Storchova and Pellman, 2004; Weaver and Cleveland, 2006; Hanahan and Weinberg, 2011), suggesting that it may potentially promote different stages of cancer evolution. To support this notion, the presence of specific

This article was published online ahead of print in MBoC in Press (http://www.molbiolcell.org/cgi/doi/10.1091/mbc.E18-10-0626) on October 31, 2018.

†These authors contributed equally to this work.

The authors declare that they have no potential conflicts of interest.

‡Present address: Genome Institute of Singapore, Agency for Science, Technology and Research (A*STAR), Singapore.

Author contributions: Z.T., Y.J.A.C., Y.J.K.C., D.C., and G.R. conceived and designed experiments. Z.T., Y.J.A.C., Y.J.K.C., and S.D.R. performed experiments. Z.T., Y.J.A.C., Y.J.K.C., S.D.R., and G.R. analyzed the data. Z.T., Y.J.A.C., Y.J.K.C., and N.P. performed statistical analysis. Z.T., Y.J.A.C., and G.R. wrote the manuscript. Y.J.A.C. and G.R. revised the manuscript. All authors have read the manuscript and agree to its content.

*Address correspondence to: Giulia Rancati (giulia.rancati@imb.a-star.edu.sg).

Abbreviations used: APC/C, anaphase-promoting complex/cyclosome; DMSO, dimethyl sulfoxide; DOX, doxorubicin; M cells, mitotic cells; M phase, mitotic phase; SAC, spindle assembly checkpoint.

aneuploid chromosomes has been shown to increase genomic instability (Zhu *et al.*, 2012; Nicholson *et al.*, 2015) and drug resistance (Lee *et al.*, 2011) as well as to provide increased growth and tumorigenic potential (Ben-David *et al.*, 2014; Rutledge *et al.*, 2016). While karyotypic changes have been hypothesized to fuel cancer evolution by bringing about haploinsufficiency and triplosensitivity of tumor suppressors and oncogenes, respectively (Davoli *et al.*, 2013), chromosome instability has been show to promote tumor relapse and improved cellular fitness (Sotillo *et al.*, 2010; Sheltzer *et al.*, 2017). At the same time, polyploidy has been shown to promote tumorigenesis (Fujiwara *et al.*, 2005), drug resistance (Kuznetsova *et al.*, 2015), and genome instability (Ganem *et al.*, 2009; Silkworth *et al.*, 2009; Kuznetsova *et al.*, 2015). While it comes as no surprise that karyotypic heterogeneity is an indicator of poor prognosis for cancer patients (Swanton *et al.*, 2009; Danielsen *et al.*, 2016), the underlying mechanisms generating such variation have not been fully elucidated.

Karyotypic instability is known to result from mutations that increase mitotic defects (Bakhoum *et al.*, 2009; Ganem *et al.*, 2009; Silkworth *et al.*, 2009) or prevent their correction (Cahill *et al.*, 1998; Sotillo *et al.*, 2010; Targa and Rancati, 2018). In the latter case, alteration of the spindle assembly checkpoint (SAC) signaling cascade, an evolutionarily conserved mechanism that delays anaphase onset by preventing the activation of the anaphase-promoting complex/cyclosome (APC/C) and the degradation of cyclin B1 (Musacchio, 2015) in response to spindle defects, was linked to chromosome instability in murine models, in a subset of colorectal cancers, and in a rare genetic disorder characterized by multiple mosaic aneuploidies (Cahill *et al.*, 1998; Hanks *et al.*, 2006; Giam and Rancati, 2015). However, genetic mutations of SAC components other than BubR1 are uncommon in cancer cells (Kops *et al.*, 2005; Solimini *et al.*, 2012), suggesting that other, perhaps nongenetic, mechanisms could promote karyotypic heterogeneity. Accordingly, karyotypic changes have been linked to exogenous factors, such as exposure to DNA-damaging agents (Bakhoum *et al.*, 2014), the presence of oxidative stress (Gentric *et al.*, 2015), viral infection (Machida *et al.*, 2009), or as a consequence of mitotic slippage in response to prolonged mitotic arrest (Rieder and Maiato, 2004). In agreement with the idea that environmental stress could lead to karyotypic heterogeneity, unicellular eukaryotes were recently shown to undergo aneuploidization and loss of heterozygosity in response to heat stress or antifungal drug treatment (Forche *et al.*, 2011; Chen *et al.*, 2012a).

Tumor microenvironments are notoriously stressful. Stresses include nutrient deprivation, hypoxia, acidic pH (Fukumura and Jain, 2007), immune surveillance (Dunn *et al.*, 2004), and heat if hyperthermia is locally or systemically applied during chemotherapy (Wust *et al.*, 2002; Jha *et al.*, 2016). In the last case, while several clinical trials and studies on bladder, head and neck, melanoma, sarcoma, esophageal, cervix, and rectal cancer have shown mixed results on potential cancer patient benefits (Cihoric *et al.*, 2015; Jha *et al.*, 2016), several clinics currently offer hyperthermia treatment to cancer patients. In some cases, hyperthermia has been administered to younger cancer patients (Seifert *et al.*, 2016).

In this study, we tested whether in vitro tumor microenvironmental stresses can induce karyotypic changes and act as a route to karyotypic heterogeneity that does not involve mutations in gatekeeper genes. We provide experimental evidence that cells from multicellular organisms, such as chromosomally stable cancer lines, undergo karyotypic changes in response to cellular stresses. Hereafter we will refer to this phenomenon as stress-induced karyotypic instability. At the molecular level, we showed that hyperthermia, by simultaneously perturbing centrosome function and attenuating the SAC, induced mitotic exit in the absence of chromosome segregation, leading to genome doubling. Finally, we report that heat-induced tetraploid cells were on the average more resistant to a panel of commonly used chemotherapeutic compounds. Our results suggest that environmental perturbations could act as a nongenetic route for the generation of genetic and phenotypic variation in cells from multicellular eukaryotes. Also, they imply that therapeutic manipulations aiming to reduce tumor microenvironmental stresses could play an important role in curbing the emergence of drug resistance and aggressive phenotypes.

RESULTS

Hyperthermia, serum starvation, and hypoxia elicit stress in cancer cell lines

We hypothesized that exposure to environmental stress conditions present in the tumor microenvironment can promote ploidy changes resulting in the karyotypic heterogeneity observed within cancer samples. To test our hypothesis, we set out to define optimal environmental stress regimens for stressors such as hyperthermia, serum starvation, and hypoxic conditions in the karyotypically homogeneous and chromosomally stable pseudodiploid human colon carcinoma cell line HCT116 (Figure 1A). Ideal stress regimens should be long enough to elicit stress-specific cellular responses, while preventing selection of standing karyotypic variation that might have been present before the treatment. This would ensure that observed karyotypic changes resulted from mitotic errors occurred during the stress treatment. After a careful evaluation, the stress regimens detailed in Figure 1A were chosen, as they minimized the number of cell doublings and deaths (Supplemental Figure S1, A and B) occurring during the treatment, while bringing about specific cellular stress. The different regimens elicited specific changes in cell shape (Supplemental Figure S1C) and brought about expected transcriptional changes (up-regulation of HSP70 for hyperthermia, down-regulation of Ki67 for serum starvation, and up-regulation of BNIP3 for hypoxia; Supplemental Figure S1D). These results showed that the treatment regimens used in this study elicit cellular stress and expected stress-specific responses.

Mitotic defects after exposure to environmental stressors

We then asked whether the above-described stress regimens could cause mitotic defects. Because cell proliferation during stress treatments was low (Supplemental Figure S1A), mitotic defects were quantified in the cell cycle following release from stress (see *Materials and Methods* for details). This setup of stress and release mimicked the constant fluctuations in microenvironmental conditions predicted to occur in tumors and allowed us to test whether exposure to these stress conditions could have longer-term effects on cancer cells. Mitotic defects occurring in prometaphase/metaphase and/or in anaphase were significantly increased after exposure to hyperthermia and serum starvation (Figure 1, B and C), suggesting that karyotypic changes could occur as a result of exposure to these stresses.

Stress-induced changes in chromosome number and structure

To quantify karyotypic changes generated during the stress treatment, we performed cytogenetics analyses (Figure 2A) of cells retrieved in the cell cycle following release from the stress (see *Materials and Methods* for details). We found that hyperthermia significantly increased the number of tetraploid cells, while serum starvation and hypoxia caused an increase in aneuploid cells (Figure 2B and

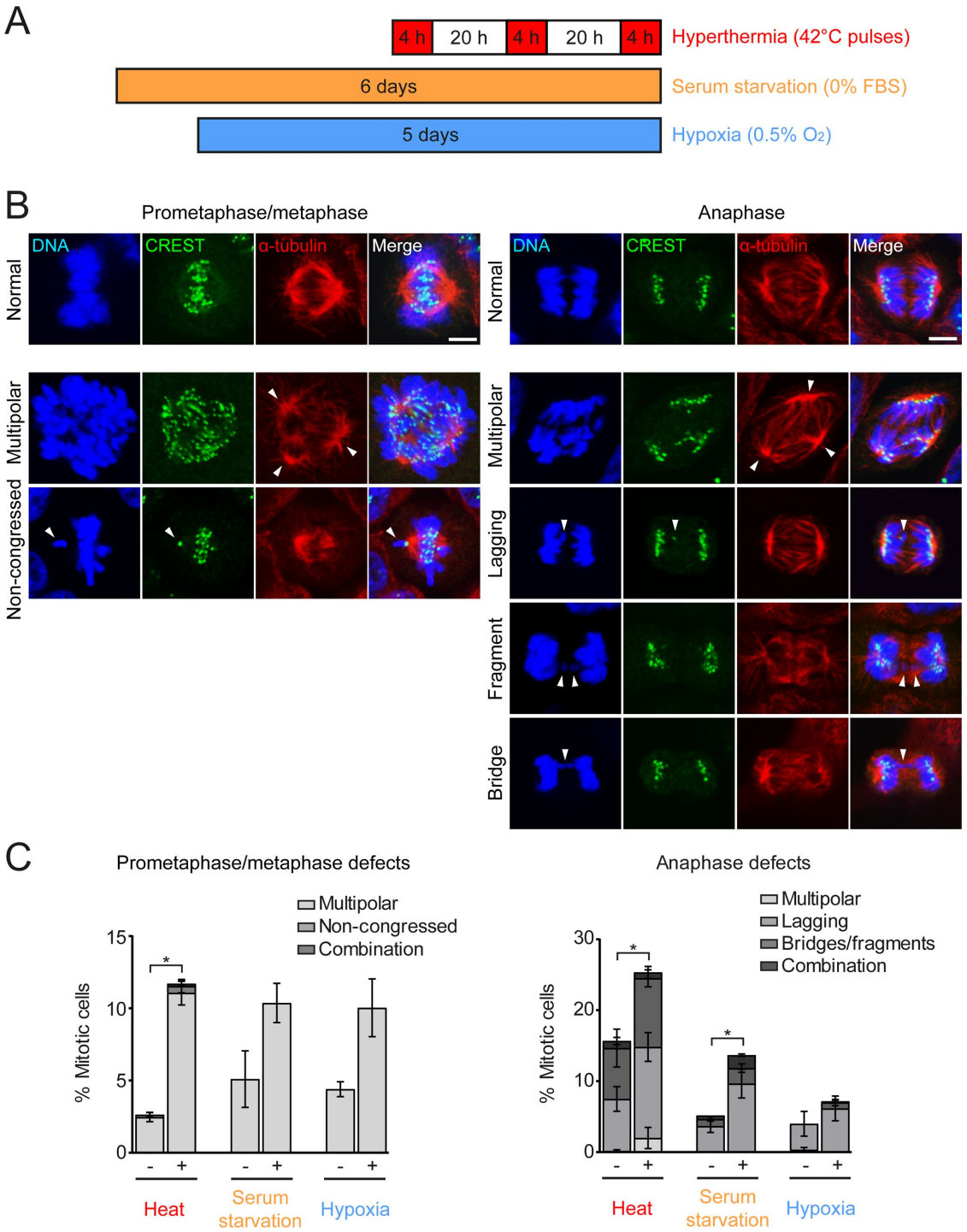

FIGURE 1: Stress regimens promote mitotic defects. (A) Diagram illustrating the stress regimens used in this study. Hyperthermia: exposure to three 4-h pulses of 42°C within 52 h; serum starvation and hypoxia: continuous absence of serum or reduced oxygen (0.5%) for 6 and 5 d, respectively. (B) Representative immunofluorescence images of mitotic errors. DNA is stained by DAPI; anti-CREST antibodies and anti–α-tubulin antibodies mark kinetochores and mitotic spindle, respectively. Arrowheads point to mitotic defects. Scale bar: 5 μm. (C) Histograms represent distributions of mitotic defects (mean ± SEM) in the indicated cell cycle phases after the indicated regimens. Mitotic defects were combined together per phase and per treatment. Significance tests were performed on the sums. *p* values (paired *t* test, two-tailed): * < 0.05. *N* = 3 biological replicates.

Supplemental Figure S2). The number of distinct chromosome counts, as well as the percentage of cells with a nonmodal chromosome number, were significantly increased under the majority of the stress conditions from those for controls (Supplemental Figure S2B), suggesting that stress induced karyotypic heterogeneity. In addition, more detailed cytogenetic analyses revealed the presence of specific defects in chromosome structure (Figure 2, C and D). Similarly to previous reports (Manning *et al.*, 2010; van Harn *et al.*, 2010), cohesion

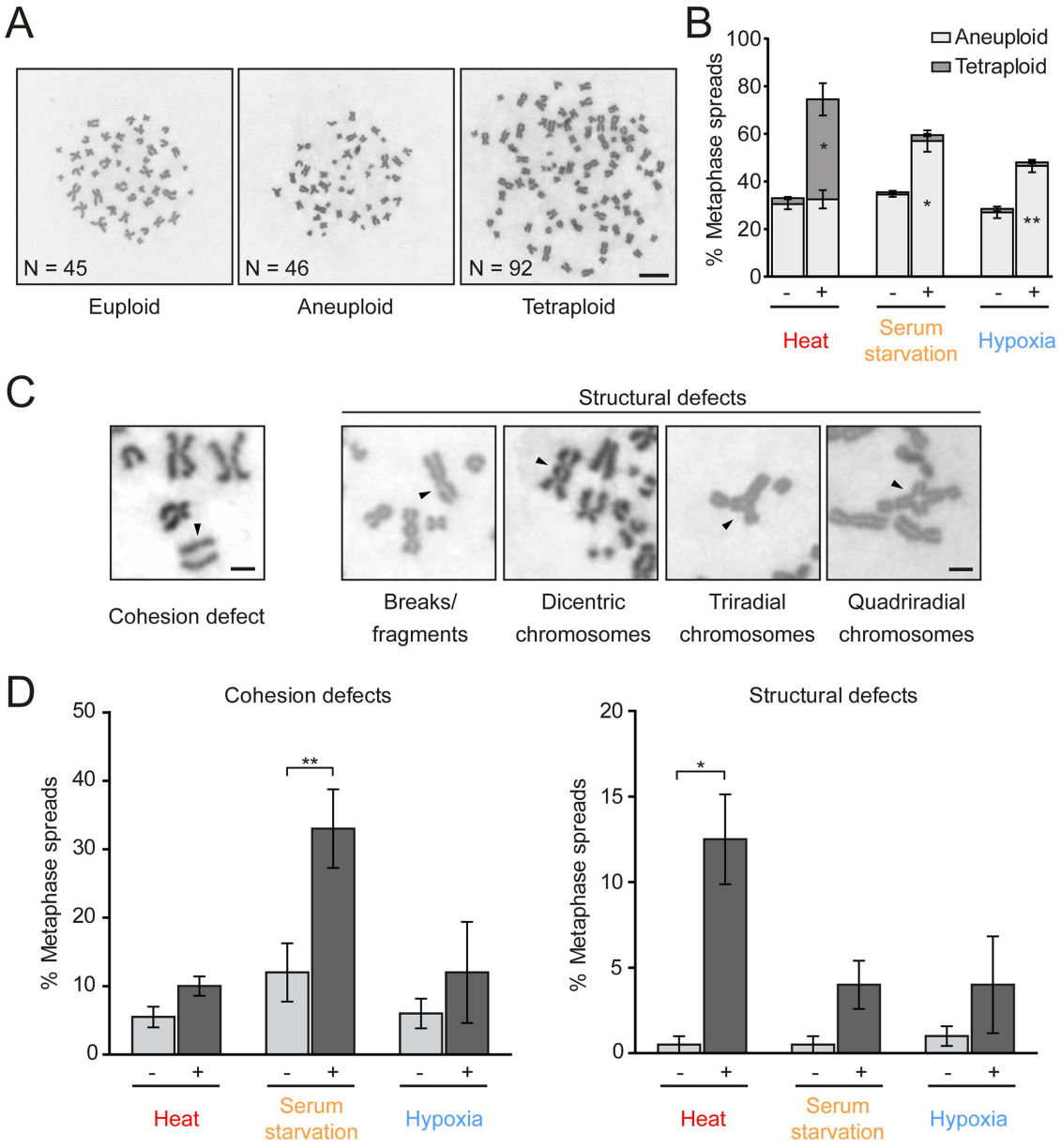

FIGURE 2: Stress regimens promote an array of karyotypic changes. (A) Representative images of HCT116 metaphase spreads. Scale bar: 10 μm. (B, D) Graphs represent mean ± SEM ($N = 3$ or 4) of ploidy changes (B) or cohesion and structural defects (D). Stress regimens are indicated at the bottom. Ploidy classification was based on chromosome counting on metaphase spreads. Euploid = 45; aneuploid ≤ 65; polyploid > 65. p values (paired t test, two-tailed): * < 0.05; ** < 0.01. (C) Representative images of cohesion and structural defects. Scale bar: 2 μm.

defects between sister chromatids were also significantly increased in serum-starved cells. Because cohesion defects have been linked to generation of aneuploidy (Holland and Cleveland, 2009), this observation suggested that loss of sister chromatid cohesion could be one of the cellular mechanisms leading to the observed increase in aneuploid cells following serum starvation. At the same time, structural defects were specifically enriched after hyperthermia treatment, consistent with prior reports that hyperthermia impacts DNA integrity (Velichko *et al.*, 2012). DNA damage specifically was present after hyperthermia but not in response to the other treatments (Supplemental Figure S3). Taken together, these observations suggest that the tested environmental stresses induced a wide array of structural and numerical chromosome changes and support a model in which stress conditions found in the tumor microenvironment can act as a nongenetic route to karyotypic heterogeneity in cancer cells.

Hyperthermia causes polyploidization in different cancer cell lines

We were intrigued by the observation that hyperthermia caused polyploidization, as heat therapy has been proposed as a promising approach to improve clinical outcomes when combined with radiation and chemotherapy and has been used in several clinical trials (van der Zee, 2002; Cihoric *et al.*, 2015). As cancer cells display large interline variability (Gascoigne and Taylor, 2008), we tested the generality of our findings by subjecting the chromosomally stable DLD1 and HCT15 cancer cell lines to the stress regimens described in Figure 1A. While hyperthermia increased the incidence of aneuploidy in DLD1 but not in HCT15 cells, it increased the fraction of tetraploid cells, as well as distinct and nonmodal karyotypes, in both cell lines (Supplemental Figure S4). At the same time, serum starvation and hypoxia treatment failed to increase the percentage of

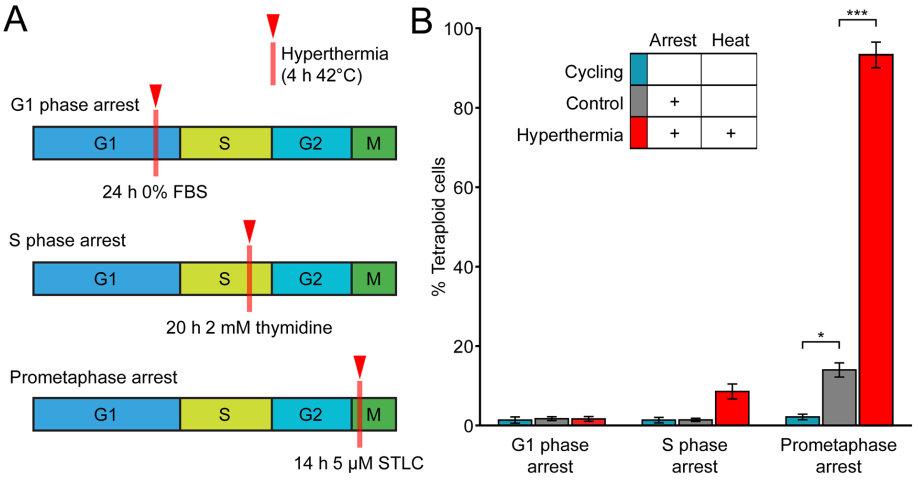

FIGURE 3: Hyperthermia-induced polyploidization in prometaphase-arrested cells. (A) Diagram depicting treatment of a single pulse of hyperthermia on G1-, S-, or prometaphase-arrested cells. Regimens used to induce cell cycle arrest are indicated. Red box with arrow: 4-h 42°C pulse. (B) Graph represents the mean ± SEM ($N = 3$) of the percentage of tetraploid HCT116 cells after the indicated treatments. Polyploidization was determined by chromosome counting after the indicated drug regimen and performed as presented in *Materials and Methods*. Top diagram color-codes presence or absence of cell cycle arrest and heat treatment in the analyzed samples. $n > 110$ cells per condition per replicate. p values (paired t test, two-tailed): * < 0.05, *** < 0.001.

aneuploid cells in either DLD1 or HCT15 cells (Supplemental Figure S4). Collectively, among all tested stressors, hyperthermia reproducibly increased the percentage of tetraploid cells across three independent cancer cell lines.

Mitotic cells are susceptible to heat-induced polyploidization

Polyploid cells arising after hyperthermia treatment had a near-tetraploid chromosome count (Supplemental Figures S2 and S4), suggesting that polyploidization most likely arose from a one-step whole-genome doubling as opposed to a gradual increase from a diploid to a tetraploid state. To understand the mechanism(s) by which hyperthermia causes polyploidization, we tested whether HCT116 cells in different cell cycle phases are differentially sensitive to hyperthermia-induced polyploidization. G1-, S-, or M- (prometaphase) arrested cells (Supplemental Figure S5) were subjected to a single 4-h, 42°C hyperthermia pulse (Figure 3A), and chromosomes were counted in the cell cycle following release from the arrest. We found that hyperthermia applied to *S*-trityl-L-cysteine (STLC)-arrested M-phase cells, but not to G1- or S-phase cells, significantly increased the percentage of tetraploid cells (Figure 3B). Qualitatively similar polyploidization rates were also observed when heat was applied to nocodazole-arrested M-phase cells (Supplemental Figure S6). These results indicate that polyploidization in response to heat results from dysregulation of mitotic events.

Hyperthermia induces mitotic exit in the absence of chromosome segregation

To visualize the mitotic events leading to polyploidization in response to hyperthermia, chromosome condensation and dynamics were imaged in an H2B-GFP HCT116 cell line (Supplemental Figure S7, A–D, and Supplemental Video S1). After ensuring that prolonged imaging did not affect mitotic length (Supplemental Figure S8A) and that the desired sample temperatures could be reliably achieved and maintained during image acquisition (Supplemental Figure S8B), we tracked cells as they were subjected to hyperthermia for 4 h and followed them for 12 h after stress release. We found that hyperthermia increased the duration of mitosis (Figure 4A and Supplemental Figure S7B), defined as the interval from nuclear envelope breakdown (NEB) to anaphase onset. While the mitotic length was most extended during heat treatment, mitotic lengthening was still significant 8 h after release from stress. Hyperthermia also significantly increased the proportion of cells that exited mitosis without chromosome segregation ($p < 0.0001$ Fisher exact test; Figure 4B, Supplemental Figure S7E, and Supplemental Video S2). These observations suggest that hyperthermia increases polyploidization by preventing chromosome segregation while licensing mitotic exit.

Hyperthermia attenuates the SAC leading to APC/C activation

Exit from mitosis in the absence of chromosome segregation could be caused either by SAC attenuation or by mitotic slippage, a process in which cyclin B1 is slowly degraded and cells exit mitosis in the presence of an active SAC. In the former case, mitotic exit is a relatively fast process, while mitotic slippage requires several hours to occur (Brito and Rieder, 2006; Sloss *et al.*, 2016). Therefore, to distinguish between these two possibilities, we first looked at the length of mitosis during heating. As shown in Figure 4C, the mean time required for mitotic exit was significantly longer when cells exited mitosis in the absence (~256 min) than in the presence of chromosome segregation (~60 min). However, on the average, exit from mitosis in the absence of chromosome segregation occurred faster than what previously observed in HCT116 cells undergoing mitotic slippage (~500 min as shown in Gascoigne and Taylor, 2008). Moreover, cells that exited mitosis without chromosome segregation during hyperthermia treatment showed large variability in mitotic length, with some entering the next G1 with relatively fast kinetics (Figure 4C). These two observations suggested that SAC might be attenuated. To further corroborate this idea, we compared mitotic exit between prometaphase-arrested control and heated cells by looking at the kinetics of cyclin B1 degradation and dephosphorylation of histone H3 at Ser10 (phospho-H3; Hendzel *et al.*, 1997; Brito and Rieder, 2006). To this end, cells were G2-/M-arrested with nocodazole for a total of 16 h. After 12 h of nocodazole treatment, "hyperthermia" cells were shifted to 42°C and sampled until the end of the experiment. While cyclin B1 and phospho-H3 were still detectable in control cells throughout the experiment, they were almost absent in heat-treated cells (Figure 5A). Cyclin B1 degradation was, however, comparable to control cells in hypoxia-treated or serum-starved cells (Supplemental Figure S9), consistent with the observation that these regimens do not cause polyploidization. To test whether cyclin B1 degradation was mediated by APC/C activation, heat-treated cells were incubated in the presence of proTAME and Apcin, known APC/C inhibitors (Sackton *et al.*, 2014). As shown in Figure 5A, chemical inhibition of APC/C partially restores cyclin B1 and phospho-H3 stability, suggesting that mitotic exit is due to SAC attenuation and premature APC/C activation in heat-treated cells. This is not in disagreement with the observation that heat lengthens mitosis (Figure 4). Indeed, because heat-induced SAC attenuation causes an active but rather slow cyclin B degradation, we expect

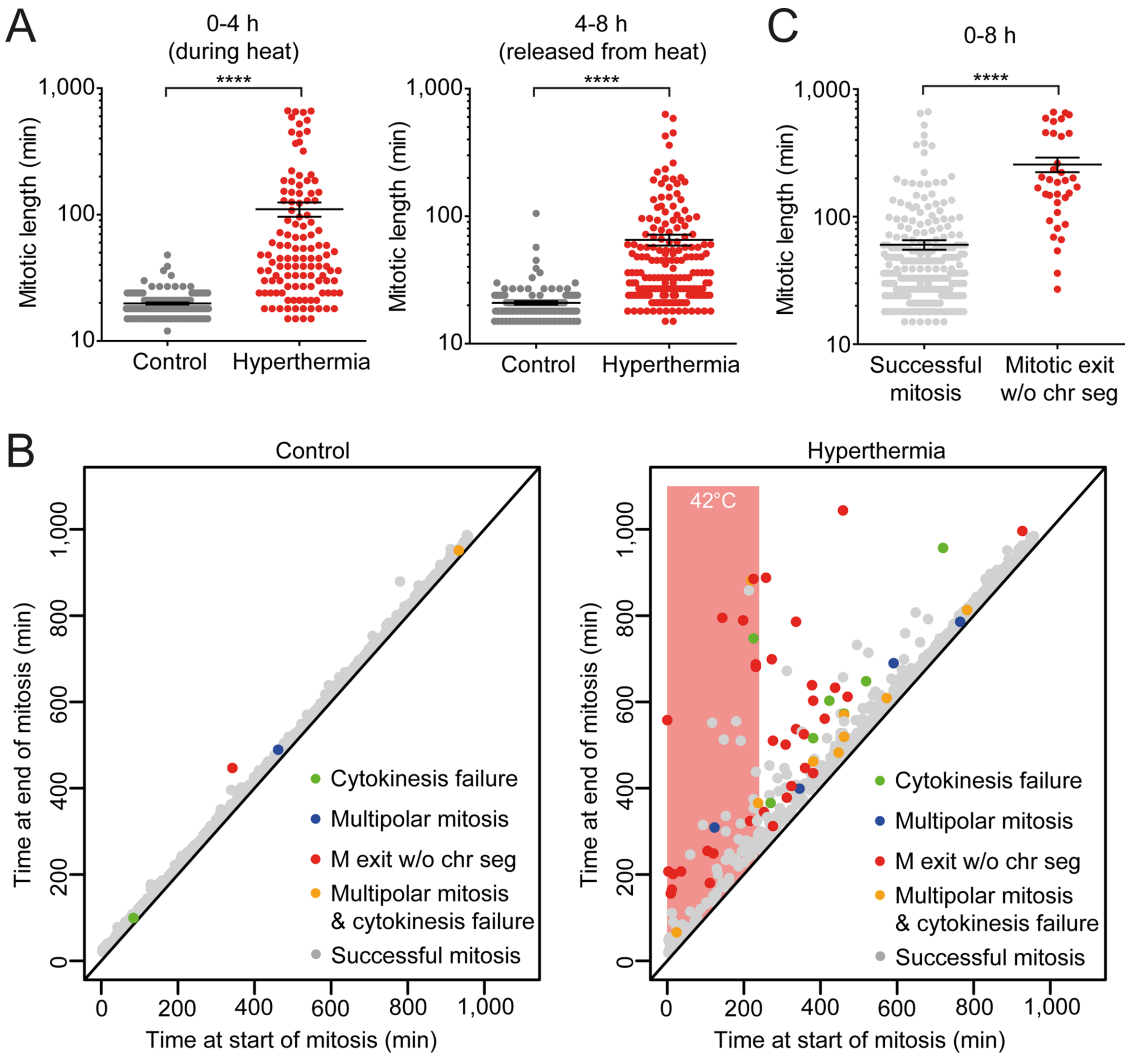

FIGURE 4: Mitotic exit in the absence of chromosome segregation in response to hyperthermia. (A) Scatterplots representing the mean ± SEM from three biological replicates of mitotic length at the indicated times during treatment (0–4 h) or after release (4–8 h). $n \geq 119$ cells per condition per time frame. *p* values (unpaired *t* test, two-tailed): **** < 0.0001. (B) Each dot represents a single cell undergoing mitosis. Successful mitosis and mitotic defects are color-coded as indicated. The position of the dot on the *x*-axis and *y*-axis reflects the time point the cell entered and exited mitosis, respectively. Because the diagonal line follows the formula $y = x$, the height above it indicates the mitotic length. The shaded red polygon (right panel) indicates the 4-h 42°C heat treatment. $n > 655$ cells per condition. Detailed quantification of mitotic defects is illustrated in Figure S7E. (C) Scatterplot with mean ± SEM from three biological replicates of mitotic length of cells treated with hyperthermia. Data points are plotted based on the cellular fate from 0 to 8 h (during and after the release from hyperthermia). For all scatterplots, mitotic length was calculated as the interval from NEB to anaphase onset. *p* values (unpaired *t* test, two-tailed): **** < 0.0001.

heat to drive a relatively quick mitotic exit in cells with low cyclin B1 levels (for instance, due to prolonged mitotic arrest; Figure 5A) while partially lengthening mitosis in cells with normal cyclin B1 levels (Figure 4C). Accordingly, localization of CENP-E and BubR1, proteins required for a full-strength mitotic checkpoint (Weaver *et al.*, 2003; Guo *et al.*, 2012), was significantly decreased from centromeres in naturally occurring (Supplemental Figure S10) and nocodazole-arrested (Figure 5, B and C) mitotic cells when heat was applied. Loss of centromere localization of CENP-E and BubR1 was not due to generalized protein degradation, as their protein levels as well as those of other SAC and mitotic proteins, did not change substantially upon heat treatment (Supplemental Figure S11, A and B). However, it has to be noted that CENP-E protein levels were slightly decreased during heat treatment. CENP-E levels as well as BubR1 phosphorylation have been shown to fluctuate during the cell cycle, peaking in G2/M and decreasing upon mitotic exit (Brown *et al.*, 1994; Taylor *et al.*, 2001; Huang *et al.*, 2008). Because heat treatment resulted in mitotic exit (Figure 5A), we argue that the decrease in CENP-E levels was due to mitotic exit rather than protein degradation. Consistently, a marked reduction in BubR1 phosphorylation appears concomitant with CENP-E protein-level reduction (Supplemental Figure S11A). Heat-induced SAC attenuation was also not the result of generalized protein folding impairment, as the interaction between key SAC components, Mad1 and Mad2, was preserved after hyperthermia (Supplemental Figure S11C). These results suggest that heat-induced mitotic exit without chromosome segregation results from attenuation of the SAC signaling cascade and APC/C-mediated cyclin B1 degradation.

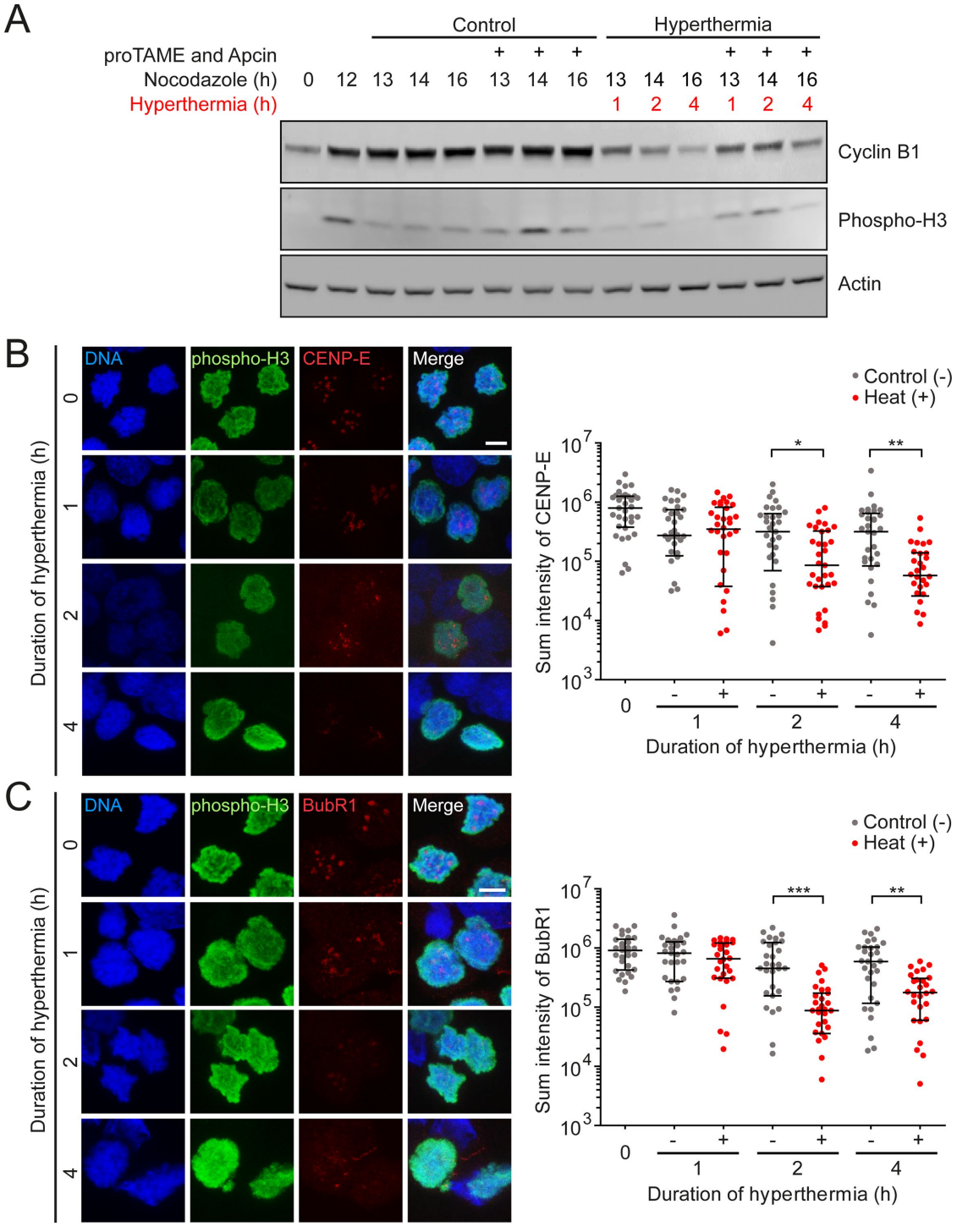

FIGURE 5: APC/C is activated in hyperthermia due to SAC attenuation. (A) Western blot of cyclin B1 and phospho-H3 on samples harvested at the indicated time points after nocodazole (100 ng/ml), APC/C inhibitors (12 μM proTAME and 25 μM Apcin) incubation, or hyperthermia treatment. Actin: loading control. (B, C) Cells were treated in nocodazole for 14 h prior to hyperthermia and were kept in nocodazole throughout the experiment. Left panels: representative IF images of kinetochore-bound CENP-E (B) or BubR1 (C) and phospho-H3, which was used to mark mitotic cells. Scale bars: 5 μm. Right panels: Quantification of CENP-E (B) or BubR1 (C) foci in mitotic cells over a 4-h time course. $n > 25$ phospho-H3-positive cells per condition per time frame. For all scatterplots, the median with interquartile range is shown. Only cells with a detectable staining are reported in the scatter plot. p values (Mann–Whitney t test, two-tailed): * < 0.05, ** < 0.01, *** < 0.001.

Hyperthermia impairs centrosome function

In response to hyperthermia treatment, we noticed that many mitotic cells slowed their cell cycle in prometaphase with chromosomes positioned in a rosette during image analysis (Supplemental Figure S7C), suggestive of bipolar spindle formation defects. While microtubules could still be substantially polymerized in interphase

and metaphase cells on exposure to heat (Supplemental Figures S12 and S13), the vast majority of mitotic cells exposed to heat assembled monopolar, multipolar, and other abnormal spindle conformations (Supplemental Figure S13). We therefore tested whether the inability to form bipolar spindles was a result of centrosome defects by quantifying centrosomal localization of γ-tubulin, a protein required for bipolar spindle formation (Raynaud-Messina *et al.*, 2004), and dynamitin, a subunit of the dynactin complex required for microtubules organization (Echeverri *et al.*, 1996). Consistent with earlier reports (Hut *et al.*, 2005; Vertii *et al.*, 2015), γ-tubulin and dynamitin localization were significantly reduced after application of hyperthermia to both interphase (Figure 6, A–C) and mitotic cells (Figure 6, D–F). Additionally, levels of Eg5, a motor protein required for the formation of bipolar spindles (Mayer *et al.*, 1999), were reduced on the spindles of mitotic cells during hyperthermia treatment (Figure 6, G and H). These hyperthermia-induced protein localization changes were protein-specific, as the levels of inner-kinetochore components (CREST; Figure 6, G and I) remained unchanged during heat. Again, they were not due to generalized protein degradation occurring at 42°C, as the protein levels of dynamitin, γ-tubulin, and Eg5 remained largely unchanged upon heat treatment (Supplemental Figure S11A). The observation that G1 and S phase–arrested cells exposed to hyperthermia divided normally without chromosome segregation defects when released from heat stress (Figure 3B) suggested that centrosome damage can be reversed. Consistently, γ-tubulin localization was gradually recovered over time after heat release, reaching control levels in ~60% of the analyzed interphase cells after 16 h (Supplemental Figure S14). Taken together, these results suggest that hyperthermia causes polyploidization by preventing chromosome segregation while licensing mitotic exit.

Tetraploid cells show increased drug resistance

Because hyperthermia therapy has been proposed to elicit increased cell death when used in conjunction with chemotherapy or radiotherapy (Wust *et al.*, 2002), we tested whether tetraploid cells can contribute to the chemotherapeutic drug resistance often seen in tumor relapses. By quantifying DNA content and chromosome number per cell (unpublished data), we isolated three HCT116 tetraploid and diploid cell lines after exposure to hyperthermia and performed clonogenic assays after treatment with a panel of chemotherapeutic or antimitotic drugs. These clones were karyotypically stable, as they maintained their ploidy throughout the entire duration of the assays (Supplemental Figure S15). Consistent with previous findings (Kuznetsova *et al.*, 2015), tetraploid lines were jointly and/or individually more resistant than diploid lines in some of the tested compounds (Figure 7 and Supplemental Figure S16). Moreover, clonogenic assays performed with naturally occurring HCT116 tetraploid cells against doxorubicin (Supplemental Figure S17) showed qualitatively similar results. Taken together, these observations suggest that hyperthermia-induced polyploidization could contribute to the emergence of drug resistance in cancer.

DISCUSSION

Stress-induced karyotypic instability and the generation of heterogeneity in cancer cells

Previous studies have indicated that tumor microenvironmental stresses can cause genetic instability in mammalian cells, such as DNA mutations and microsatellite instability (Reynolds *et al.*, 1996; Chatterjee *et al.*, 2015). Our findings extend these observations to include large-scale genomic changes such as numerical and structural chromosomal aberrations and whole-genome doubling. We observed that while some stresses elicit different karyotypic changes in different cell lines, others such as heat treatment bring about similar genome changes regardless of the cellular genetic background. Because tumor masses are often composed of genetically heterogeneous cells, this observation suggests that even the presence of a single stress condition could have heterogeneous effects on the karyotypes of cancer cells. Moreover, the fact that aneuploidy and polyploidy themselves contribute to genomic instability (Ganem *et al.*, 2009; Silkworth *et al.*, 2009; Sheltzer *et al.*, 2011; Nicholson *et al.*, 2015) suggests that even a transient exposure to microenvironmental stresses could be sufficient to kick-start a vicious loop, generating further genetic and karyotypic variation. Last, mechanisms that increase genome instability in response to cellular stresses could represent optimal strategies for adaptation to fluctuating environments. Indeed, mutations in gatekeeper genes are predicted to cause genome instability regardless of external conditions. While this could promote adaptation to unfavorable conditions, it might also lead to a loss of fitness when the stress subsides (Chen *et al.*, 2012c). On the contrary, stress-induced genome instability is predicted to increase evolvability and thus adaptability under stressful environments while retaining genome stability and thus fitness when more favorable conditions return (Chen *et al.*, 2012b; Berman, 2016). Therefore, as proposed for single-cell eukaryotes (Chen *et al.*, 2012b), chromosome and ploidy variation after exposure to environmental stresses could also be a cellular mechanism for mammalian cells to adapt to fluctuating environments. The finding that heat-induced polyploidization is accompanied by attenuation of SAC signaling cascade suggest that cells could modulate their adaptive potential by temporarily altering pathways involved in genome stability. Identification and dissection of such mechanisms could provide novel therapeutic avenues to curb the emergence of drug resistance in cancer cells and eukaryotic pathogens alike.

Molecular mechanism of heat-induced polyploidization

Our findings suggest that hyperthermia has two effects on mitotic progression. First, hyperthermia impairs localization of dynamitin and γ-tubulin (Figure 6, A–F), essential centrosome proteins, thereby affecting centrosome function and formation of a bipolar spindle (Supplemental Figure S13). Second, in mitotic cells, hyperthermia impairs the centromeric localization of CENP-E and BubR1 (Figure 5, B and C, and Supplemental Figure S10), leading to SAC attenuation, unscheduled APC/C activation, and cyclin B1 degradation (Figure 5A). Therefore, SAC attenuation in the absence of a bipolar spindle drives cells out of mitosis and leads to polyploidization. At the molecular level, we hypothesize that heat-induced SAC attenuation is a consequence of kinetochore misfolding. As shown in Figure 5 and Supplemental Figure S11, while CENP-E and BubR1 localization are impaired during heat treatment, their protein abundance is not dramatically affected, suggesting that SAC attenuation is due the inability of cells to correctly localize some SAC proteins rather than generalized protein degradation. Supporting our hypothesis, Hsp90 activity is required for inner kinetochore folding in both budding yeast (Stemmann *et al.*, 2002; Chen *et al.*, 2012b) and mammalian cells (Davies and Kaplan, 2010). Therefore, we speculate that heat treatment titrates Hsp90 activity, leading to kinetochore misfolding, BubR1 and CENP-E mislocalization, and ultimately SAC attenuation.

We also would like to clarify that heat-induced polyploidization is likely not due to generalized protein degradation or failure to assemble the mitotic machinery. First, cells still retain their overall ability to assemble microtubules, mitotic structures, though aberrant,

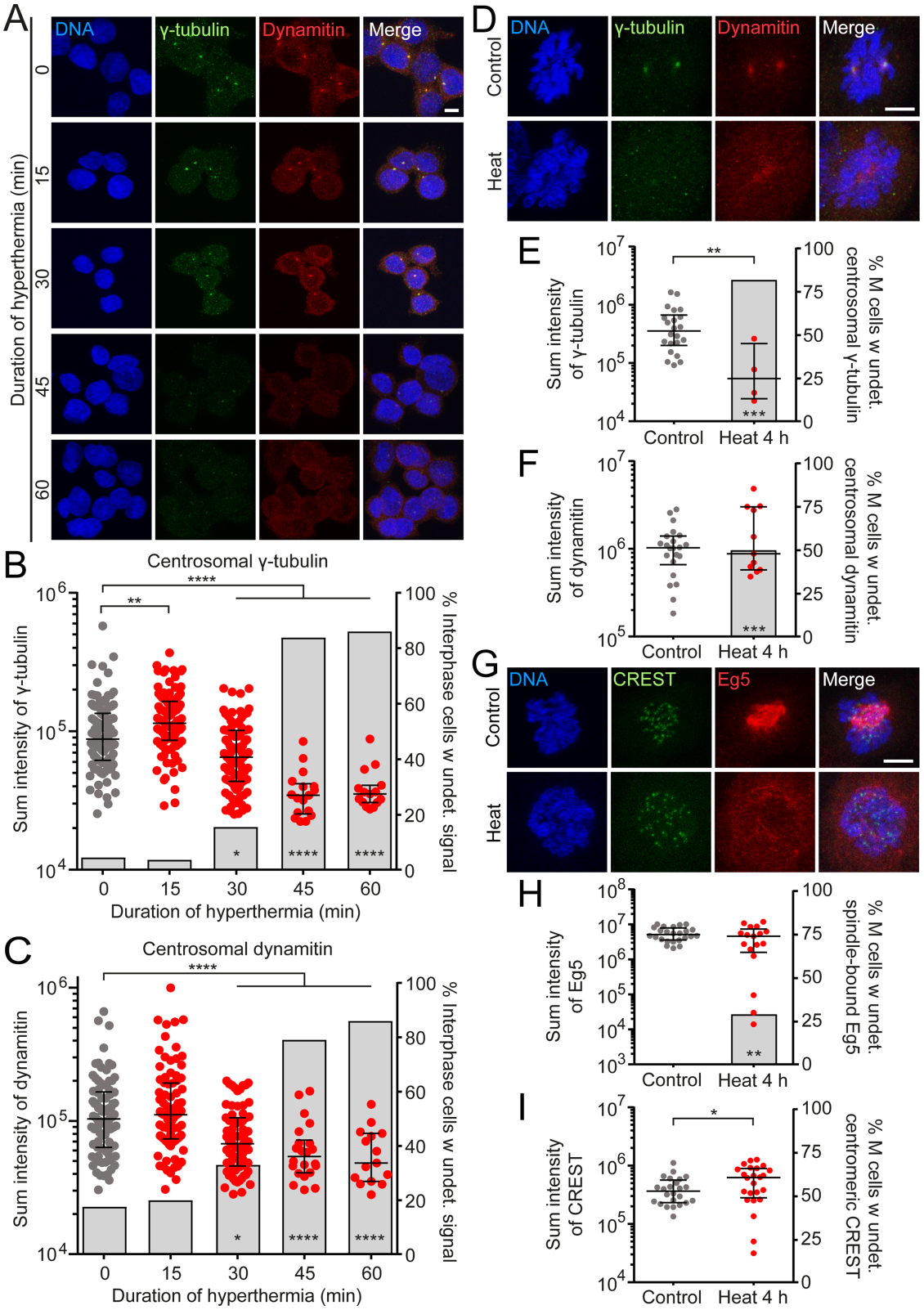

FIGURE 6: Mislocalization of centrosome components upon heat treatment. (A, D) Representative immunofluorescence images of γ-tubulin (green) and dynamitin (red) localization at the centrosomes of interphase (A) or mitotic (D) cells at indicated time points after the beginning of heat treatment. Scale bars: 5 μm. (B, C) Left *y*-axis: quantification of γ-tubulin (B) and dynamitin (C) foci as sum intensity of detectable spots at the centromeres during interphase. Right *y*-axis: percentage of interphase cells with undetectable centrosomal γ-tubulin (B) and dynamitin (C) from (A). $n \geq 100$ interphase cells per time point. (E, F) Left *y*-axis: quantification of γ-tubulin (E) and dynamitin (F) foci as sum intensity of detectable spots at the centromeres during prometaphase. Right *y*-axis: percentage of mitotic cells with undetectable centrosomal γ-tubulin (E) and dynamitin (F) from D. $n > 20$ mitotic cells per condition. (G) Representative

and inner kinetochores during heat treatment (Supplemental Figures S12 and S13 and CREST localization in Figure 6, G and I). Second, mitotic proteins and structures are still in their active conformations. Indeed, protein levels of many SAC and mitotic proteins (BubR1, CENP-E, Eg5, dynamitin, β- and γ-tubulin, Mad1, and Mad2) are largely unchanged during hyperthermia (Supplemental Figure S11, A and B). Because denatured and nonactive proteins are targeted for degradation by the unfolded protein response (Tsai and Weissman, 2010), this observation suggests that BubR1, CENP-E, Mad1, Mad2, Eg5, dynamitin, and β- and γ-tubulin maintain an active conformation under heat. Furthermore, Mad1 and Mad2 interaction is preserved under heat (Supplemental Figure S11C), suggesting that the folding of SAC proteins is not affected by the treatment. Finally, APC/C is still assembled correctly and in its active conformation, as it promotes the degradation of its natural target cyclin B1 during hyperthermia exposure (Figure 5A). These observations support the idea that mitotic proteins and machinery are in their active conformation during hyperthermia and reaffirm that the ploidy changes are likely not the result of generalized degradation of the mitotic machinery.

Implications for cancer therapy

Our results suggest that harsh tumor microenvironmental conditions could favor the generation of intratumor heterogeneity, thereby promoting drug resistance and evolution of cancer cells toward more aggressive phenotypes. Nontransformed cells halt cell cycle progression in response to aneuploidization and polyploidization by activating the tumor suppressor p53 (Ganem and Pellman, 2007). However, because the vast majority of solid tumors harbor inactivating mutations in p53 or in components of its signaling cascade (Rivlin *et al.*, 2011), aneuploid and polyploid cancer cells generated in response to environmental stresses will most likely be able to proliferate, increasing the complexity of intratumor heterogeneity. Moreover, recent evidence shows that perturbation of other oncogenes, such as cyclin D, is sufficient to restore the proliferation of tetraploid RPE cells (Potapova *et al.*, 2016), suggesting that cancer cells with an intact p53 signaling cascade have multiple routes to proliferate despite large-scale genome changes. Our data suggest that drug treatments aiming at increasing tumor microenvironmental stress conditions might actually lead to increased intratumor heterogeneity and promote the emergence of drug resistance. Mathematical models have suggested that harsh tumor microenvironments can promote the generation of invasive and aggressive traits (Anderson *et al.*, 2006). In addition, preclinical studies indicate that treatment with antiangiogenic therapy to exacerbate tumor hypoxic conditions could promote cancer aggressiveness and metastatic potential (Paez-Ribes *et al.*, 2009; Cooke *et al.*, 2012; Lu *et al.*, 2012; Sennino *et al.*, 2012; Vasudev and Reynolds, 2014).

Regional or whole body hyperthermia has been utilized to increase cell death (Wust *et al.*, 2002) and was used in 16 clinical trials as part of anticancer treatment in 2015 (Cihoric *et al.*, 2015). However, our results suggest that hyperthermia could instead increase intratumor heterogeneity and phenotypic variation and promote drug resistance. Clinical trials on a variety of several different cancer types have shown varying degrees of success of hyperthermia for cancer treatment (Jha *et al.*, 2016).The observation that heat-derived tetraploid cells are more resistant to DNA-damaging drugs but more sensitive to spindle-depolymerizing agents (Figure 7B) suggests that application of hyperthermia in clinical oncology should be combined with the use of antimitotic drugs that disrupt the microtubule spindle.

MATERIALS AND METHODS

Cell lines, cell culture, and chemicals

Colorectal carcinoma cell lines HCT116 (CCL-247), HCT15 (CCL-225), and DLD1 (CCL-221) were obtained from the American Type Culture Collection (Manassas, VA) and were cultured under standard conditions unless otherwise specified. Nocodazole (M1404; Sigma-Aldrich, St. Louis, MO) was used for G2/M arrest. KaryoMAX Colcemid (15212012; Life Technologies, Thermo Fisher Scientific, Waltham, MA) was used for metaphase spread preparation. proTAME (I-440-01M; R&D Systems, Minneapolis, MN) and Apcin (I-444-05M; R&D Systems) were used for APC/C inhibition. pBabe-H2B-GFP was obtained from P. Mathijs Voorhoeve.

For cell cycle arrest experiments, G1-, S-, or prometaphase arrests were achieved by incubating HCT116 cells in serum-deprived medium for 24 h, in 2 mM thymidine (T1895; Sigma-Aldrich) for 20 h, or with 5 µM STLC (164739; Sigma-Aldrich) for 14 h, respectively. Heated cells were then exposed to 42°C for 4 h while still arrested. Fluorescence-activated cell sorting (FACS) analysis was conducted before the arrest and during the arrest, both before and after stress (refer to Supplemental Methods in the Supplemental Material).

Stress regimens

For the different stress regimens, cells were plated as following: 5×10^4 for hypoxia, 5×10^5 for hyperthermia, and 1×10^6 for serum starvation. For hypoxia stress (0.5% O_2, 5% CO_2), cells were incubated in a humidified hypoxia chamber (BioSpherix, Parish, NY). For hyperthermia stress, cells were shifted to a preheated incubator that was kept at a constant 42°C and 5% CO_2. For serum starvation, cells were grown in their respective media devoid of FBS. Samples to assess mitotic defects or karyotypes were harvested 1 d after cells were returned to standard conditions. If cells were confluent at the end of the stress regimens, both control and stressed cells were passaged to ensure a higher mitotic index at the time of harvesting.

immunofluorescence images of CREST (green) and Eg5 (red) mitotic cells after a single pulse of 42°C for 4 h. Scale bar: 5 µm. (H, I) Left *y*-axis: quantification of Eg5 (H) and CREST (I) foci as sum intensity of detectable structures or spots in the cell during prometaphase. Right *y*-axis: percentage of mitotic cells with undetectable spindle-bound Eg5 (H) and centromeric CREST (I). $n > 20$ mitotic cells per condition. In B and C, E and F, and H and I, *p* values at the bottoms of bar graphs refer to the absence of the indicated protein with respect to 0 min/control (Fisher's exact *t* test, two-tailed): * < 0.05, ** < 0.01, *** < 0.001, **** < 0.0001. For all scatterplots, the median with interquartile range is shown and *p* values on top of plots (Mann–Whitney *t* test, two-tailed): * < 0.05, ** < 0.01, **** < 0.0001. Only cells with a detectable staining are reported in the scatterplot. Experiments were performed in duplicates with qualitatively similar results. In D–I, cells were presynchronized in the S-phase using thymidine and released in fresh media 4 h before treatment to enrich for mitotic events.

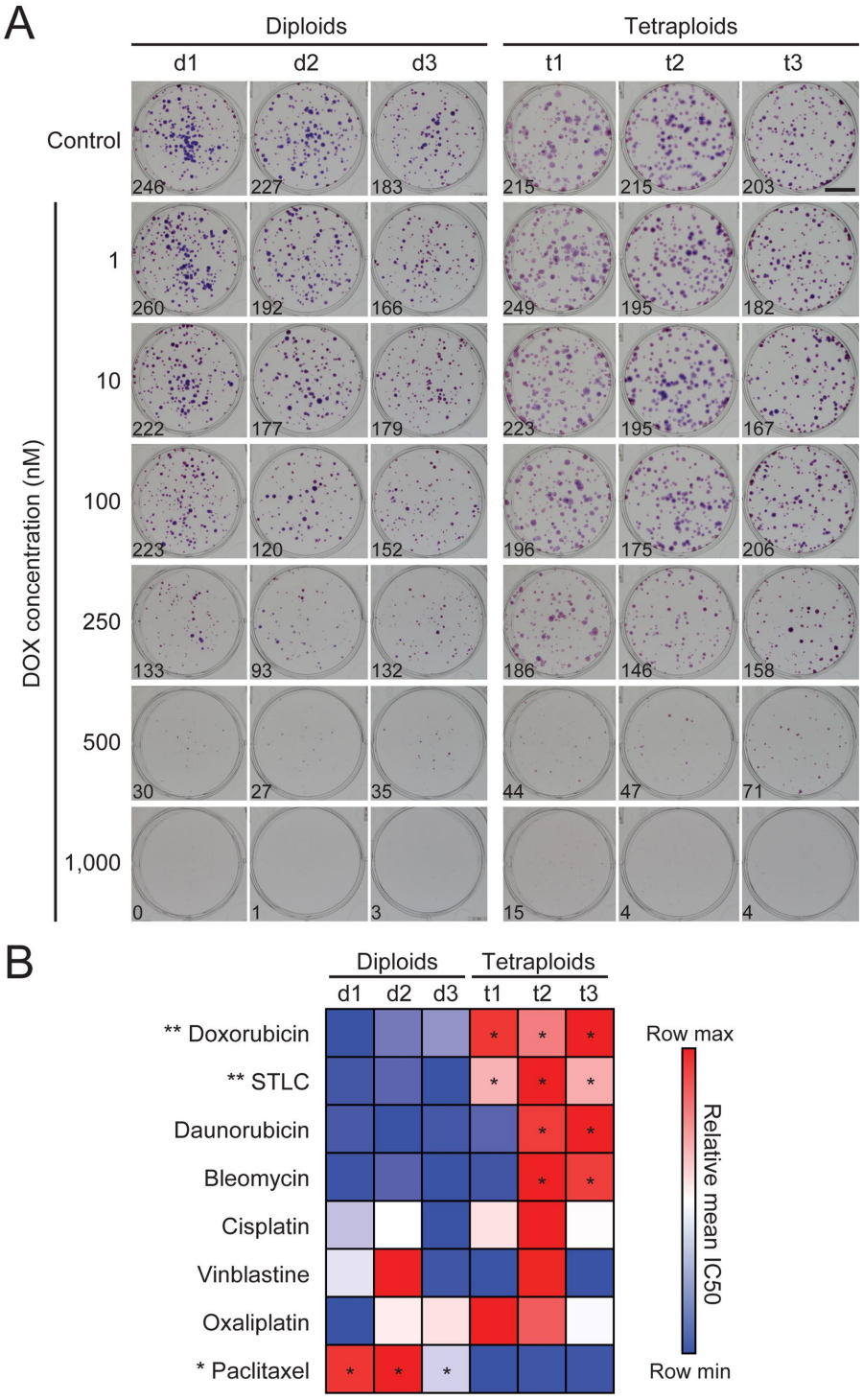

FIGURE 7: Heat-induced tetraploid clones show increased resistance to several chemotherapeutic drugs. (A) Representative diploid and tetraploid clonogenic plates after doxorubicin (DOX) treatment and control (DMSO). The number of colonies present in each condition is indicated in the bottom left of each panel. Scale bar: 1 cm. (B) Heat map of the relative mean IC50 of heat-induced diploid or tetraploid clones after the indicated drug treatments. $N = 2$ biological replicates. Each row was normalized independently and displayed using Morpheus software (Broad Institute; https://software.broadinstitute.org/morpheus/). Group significance per drug was calculated using a two-tailed *t* test (* < 0.05, ** < 0.01) based on the average IC50 of all tetraploid versus all diploid clones and displayed to the left of the drug name. Individual tetraploid clone significance was calculated as *Z*-scores with respect to the IC50 mean of all diploid clones per drug. In the case of paclitaxel, individual diploid clone significance was calculated as *Z*-scores instead. A *Z*-score > 3 was considered statistically significant and is represented as * in the box. IC50 values of individual clones are available in Supplemental Figure S16.

Antibodies

Western blot and immunofluorescence: cyclin B1 (4138S; Cell Signaling, Danvers, MA), phospho-histone-H3 (pSer10) (H0412; Sigma-Aldrich), actin (ab8226; Abcam, Cambridge, UK), dynamitin (611002; BD Biosciences, Franklin Lakes, NJ), α-tubulin (T9026; Sigma-Aldrich), γ-tubulin (T3559; Sigma-Aldrich), BubR1 (IF: ab4637; Abcam) (WB: 612502; BD Biosciences), CENP-E (IF: ab5093; Abcam) (WB: ab133583; Abcam), CREST (15-234-0001; Antibodies Inc., Davis, CA), 53BP1 (sc-22760; Santa Cruz, Dallas, TX), γ-H2AX (05-636; Upstate), Eg5 (ab181981; Abcam). Secondary antibodies (all from Molecular Probes, Eugene, OR): goat anti-human Alexa488 (A11013), goat anti-mouse Alexa488 (A11001), goat anti-mouse Alexa594 (A11005), and goat anti-rabbit Alexa568 (A11011). Western blots were acquired on an Odyssey Infrared Imaging System (Li-Cor, Lincoln, NE) using standard procedures. mFISH probes (24XCyte, D-0125-060-DI; MetaSystems, Altlussheim, Germany) were hybridized following the manufacturer's protocol.

Microscopy

Metaphase spreads either were visualized with AxioImager Z1 (Carl Zeiss, Oberkochen, Germany) and images taken with either an AxioCam MRm (Carl Zeiss) or a CoolSNAP HQ2 CCD camera (Photometrics, Tucson, AZ), or were visualized with DM6000 B (Leica, Wetzlar, Germany) and images taken with CV-M2CL (JAI, Yokohama, Japan), or were visualized with Imager.Z2 (Carl Zeiss) and images taken with CoolCube 1 (MetaSystems). For each time interval and condition, images were captured from a field of view with clear 4′,6-diamidino-2-phenylindole (DAPI) (Sigma-Aldrich) staining and the cells were analyzed sequentially subsequently, starting from the first captured image, with noise manually excluded, until the specified number of cells to minimize bias was achieved.

Live-cell imaging

Live-cell imaging was performed on an IX83 (Olympus, Tokyo, Japan) that was fitted with a Tokai Hit INUG2E-ZILCS (stage top heater and CO_2 controller) and an INUB-SFBP (stage heater) to maintain 5% CO_2 concentration and perform the temperature changes. Images were taken at 3-min intervals. For the live-cell imaging experiments reported in Figure 4, heat-treated cells do not form a metaphase plate, as their chromosomes are arrayed in a doughnut shape typical of cells arrested with microtubule motor inhibitors. Mitotic exit without

chromosome segregation is scored for mitotic cells that underwent chromosome decondensation without any sign of chromosome segregation. Because we were unable to observe any distinct and apparent chromosome movement during the imaging, chromosome segregation defects were not included in the analysis.

Immunofluorescence analysis

ImageJ was used for analysis and Imaris 8 software (Bitplane, Belfast, UK) was used for three-dimensional visualization and quantification. The Imaris Contour Surface tool was first used to create surfaces based on local contrast thresholds (including surface smoothing and background subtraction). Surfaces were then filtered based on volume (voxels) to further minimize noise, and the total fluorescence intensity (sum pixel intensity) was quantitated for each cell. To remain unbiased, the same thresholding was used in each experiment. Cells in which the immunofluorescence signal was below the set threshold were classified as "cells w undet." corresponding protein in Figure 6 and Supplemental Figures S10 and S14.

Clonogenic assay

To generate heat-induced clones, cells were first incubated at 42°C for 4 h over three consecutive days and then single-cell sorted (FACSAria II; BD Biosciences) based on cell size into individual wells in 96-well plates with 50% conditioned media. After ~2–3 wk of incubation, colonies were harvested and their ploidy was analyzed by FACS and metaphase spreads. For each drug treatment, two biological replicates with two technical replicates per clone was conducted. Four hundred cells/well were plated a day before they were subjected to the indicated drug treatments for 3 h. After 1 wk of incubation under standard conditions, cells were ethanol-fixed and stained using 0.05% crystal violet (C3886; Sigma-Aldrich). Counting was performed manually. Drugs: bleomycin (ab142977; Abcam), cisplatin (ab141398; Abcam), daunorubicin (D0125000; Sigma-Aldrich), doxorubicin (D1515; Sigma-Aldrich), oxaliplatin (ab141054; Abcam), STLC (164739; Sigma-Aldrich), paclitaxel (T7402; Sigma-Aldrich), vinblastine (V1277; Sigma-Aldrich). All drugs were dissolved in dimethyl sulfoxide (DMSO) (D2650; Sigma-Aldrich) except cisplatin, which was dissolved in saline.

Metaphase spreads

Cells were harvested by trypsinization and washed once in phosphate-buffered saline (PBS). Cells were resuspended gently in ~100 µl of PBS, and 75 mM potassium chloride (Kanto Chemical, Tokyo, Japan) was added slowly up to a volume of 10 ml. The samples were then incubated for 10 min in a 37°C water bath. Following that, 1 ml of Carnoy solution (3:1 methanol:acetic acid) was added to each sample, and samples were centrifuged for 10 min at 1000 rpm. Supernatant was discarded and cells were gently resuspended in a small amount of the remaining supernatant. Carnoy solution (10 ml) was added slowly to the samples and cells were fixed for at least 1 h at room temperature (RT). Samples were centrifuged for 10 min at 1000 rpm, supernatant was discarded, and cells were fixed again with 10 ml of fresh Carnoy for at least 1 h at RT. Samples were then centrifuged and pellets were resuspended in a suitable volume (~0.5–1.5 ml) of Carnoy solution. A sample of 20 µl of this suspension was drawn up and dropped from a height (10–30 cm) onto glass slides and allowed to air-dry. DNA was then stained with Giemsa (Life Technologies, Thermo Fisher Scientific).

Western blot

Cells were harvested through trypsinization and washed 1× with PBS, and cell pellets were snap-frozen in liquid nitrogen. Cells were then lysed with RIPA buffer (Thermo Fisher Scientific) supplemented with cOmplete protease inhibitors (Roche, Basel, Switzerland) and phosphatase inhibitors (Nacalai Tesque). Total protein was measured with a Quick Start Bradford assay (Bio-Rad, Hercules, CA) and boiled at 95°C for 5 min before being resolved in 4–15% Mini-PROTEAN TGX Precast Gel (Bio-Rad) at 100 V, 100 min. Resolved proteins were then transferred onto 0.2 µm nitrocellulose membrane (Thermo Fisher Scientific) at 100 V, 60 min. Membranes were blocked in Odyssey Blocking Buffer (Li-Cor) and probed with respective primary antibodies, overnight at 4°C. Membranes were washed three times for 5 min with Tris-buffered saline (1st Base) + 0.05% Tween 20 (Sigma-Aldrich). IRDye 680RD and 800CW IgG (H+L) (Li-Cor) were used as secondary detection reagents, and imaging was done on an Odyssey Infrared Imaging System (Li-Cor). Images were cropped in Adobe Photoshop and levels were minimally adjusted. A quantity of 30 µg of protein was loaded per well.

Immunofluorescence preparation and image acquisition

Cells cultured on 22 × 22 mm glass coverslips (Paul Marienfeld, Lauda-Königshofen, Germany) in six-well plates (Nunc, Thermo Fisher Scientific) were washed with PBS and fixed either with 4% freshly made formaldehyde for 30 min at RT or with 100% ice-cold methanol for 10 min. Formaldehyde-fixed cells were then permeabilized with 0.25% Triton X-100 in PBS for 10 min at RT; no further permeabilization was performed for methanol-fixed cells. All cells were then washed and incubated in blocking buffer (5% normal goat serum [Santa Cruz], 2% bovine serum albumin [PAA Laboratories, Austria], 0.1% Triton X-100 [USB Corporation, Cleveland, OH] in PBS) for 1 h and incubated with the respective primary antibodies in blocking buffer overnight at 4°C. Following washing, cells were incubated with conjugated secondary antibodies in blocking buffer for 1 h at RT, washed, and mounted with 1 µg/ml DAPI. α-Tubulin images were captured using a FV3000 RS inverted confocal microscope with UPLSAPO 60× NA 1.35 objective (all from Olympus) at zoom level 1.0 and step size 0.55 µm. All other images were captured using an FV1000 confocal laser scanning microscope either with PLAPO 100× NA 1.45 or with UPLSAPO 100× NA 1.40 objective (all from Olympus) at 1.3 zoom level. Optical sections were taken sequentially for each channel along the *z*-axis using a step size of 0.52 µm.

Statistical analysis

Prism or Excel was used for statistical analyses. Biological replicates are referred to as "*N*"; number of cells analyzed within each experiment is referred to as "*n*." Experimental data are represented as mean ±standard error of the mean (SEM). The median with interquartile range is shown in scatterplots. The two-tailed Student's *t* test or Fisher exact *t* test was used as indicated. Results were considered statistically significant if the p value < 0.05.

ACKNOWLEDGMENTS

We thank the Rancati and Pavelka labs for helpful discussions, Mathijs Voorhoeve for the pBabe-H2B-GFP plasmid, Graham Wright and members of the IMB Microscopy Unit for their assistance and advice, and Anna De Antoni from the FIRC Institute of Molecular Oncology for the coimmunoprecipitation advice. This study was funded by an A*STAR Investigatorship (Ref. No. 1437a00119) awarded to G.R. Work in the Cimini lab was partly supported by National Science Foundation grant MCB-1517506.

REFERENCES

Anderson AR, Weaver AM, Cummings PT, Quaranta V (2006). Tumor morphology and phenotypic evolution driven by selective pressure from the microenvironment. Cell 127, 905–915.

Bakhoum SF, Kabeche L, Murnane JP, Zaki BI, Compton DA (2014). DNA-damage response during mitosis induces whole-chromosome missegregation. Cancer Discov 4, 1281–1289.

Bakhoum SF, Thompson SL, Manning AL, Compton DA (2009). Genome stability is ensured by temporal control of kinetochore-microtubule dynamics. Nat Cell Biol 11, 27–35.

Ben-David U, Arad G, Weissbein U, Mandefro B, Maimon A, Golan-Lev T, Narwani K, Clark AT, Andrews PW, Benvenisty N, Carlos Biancotti J (2014). Aneuploidy induces profound changes in gene expression, proliferation and tumorigenicity of human pluripotent stem cells. Nat Commun 5, 4825.

Berman J (2016). Ploidy plasticity: a rapid and reversible strategy for adaptation to stress. FEMS Yeast Res 16, fow020.

Brito DA, Rieder CL (2006). Mitotic checkpoint slippage in humans occurs via cyclin B destruction in the presence of an active checkpoint. Curr Biol 16, 1194–1200.

Brown KD, Coulson RM, Yen TJ, Cleveland DW (1994). Cyclin-like accumulation and loss of the putative kinetochore motor CENP-E results from coupling continuous synthesis with specific degradation at the end of mitosis. J Cell Biol 125, 1303.

Burrell RA, McGranahan N, Bartek J, Swanton C (2013). The causes and consequences of genetic heterogeneity in cancer evolution. Nature 501, 338–345.

Cahill DP, Lengauer C, Yu J, Riggins GJ, Willson JK, Markowitz SD, Kinzler KW, Vogelstein B (1998). Mutations of mitotic checkpoint genes in human cancers. Nature 392, 300–303.

Chatterjee N, Lin Y, Santillan BA, Yotnda P, Wilson JH (2015). Environmental stress induces trinucleotide repeat mutagenesis in human cells. Proc Natl Acad Sci USA 112, 3764–3769.

Chen CP, Su YN, Weng SL, Tsai FJ, Chen CY, Liu YP, Chern SR, Chen WL, Wu PC, Wang W (2012a). Rapid aneuploidy diagnosis of trisomy 18 by array comparative genomic hybridization using uncultured amniocytes in a pregnancy with fetal arachnoid cyst detected in late second trimester. Taiwan J Obstet Gynecol 51, 481–484.

Chen G, Bradford WD, Seidel CW, Li R (2012b). Hsp90 stress potentiates rapid cellular adaptation through induction of aneuploidy. Nature 482, 246–250.

Chen G, Rubinstein B, Li R (2012c). Whole chromosome aneuploidy: big mutations drive adaptation by phenotypic leap. Bioessays 34, 893–900.

Cihoric N, Tsikkinis A, van Rhoon G, Crezee H, Aebersold DM, Bodis S, Beck M, Nadobny J, Budach V, Wust P, Ghadjar P (2015). Hyperthermia-related clinical trials on cancer treatment within the ClinicalTrials.gov registry. Int J Hyperthermia 31, 609–614.

Cooke VG, LeBleu VS, Keskin D, Khan Z, O'Connell JT, Teng Y, Duncan MB, Xie L, Maeda G, Vong S, *et al.* (2012). Pericyte depletion results in hypoxia-associated epithelial-to-mesenchymal transition and metastasis mediated by met signaling pathway. Cancer Cell 21, 66–81.

Danielsen HE, Pradhan M, Novelli M (2016). Revisiting tumour aneuploidy—the place of ploidy assessment in the molecular era. Nat Rev Clin Oncol 13, 291–304.

Davies AE, Kaplan KB (2010). Hsp90–Sgt1 and Skp1 target human Mis12 complexes to ensure efficient formation of kinetochore–microtubule binding sites. J Cell Biol 189, 261.

Davoli T, Xu AW, Mengwasser KE, Sack LM, Yoon JC, Park PJ, Elledge SJ (2013). Cumulative haploinsufficiency and triplosensitivity drive aneuploidy patterns and shape the cancer genome. Cell 155, 948–962.

Dunn GP, Old LJ, Schreiber RD (2004). The immunobiology of cancer immunosurveillance and immunoediting. Immunity 21, 137–148.

Echeverri CJ, Paschal BM, Vaughan KT, Vallee RB (1996). Molecular characterization of the 50-kD subunit of dynactin reveals function for the complex in chromosome alignment and spindle organization during mitosis. J Cell Biol 132, 617–633.

Forche A, Abbey D, Pisithkul T, Weinzierl MA, Ringstrom T, Bruck D, Petersen K, Berman J (2011). Stress alters rates and types of loss of heterozygosity in *Candida albicans*. MBio 2, e00129-11.

Fujiwara T, Bandi M, Nitta M, Ivanova EV, Bronson RT, Pellman D (2005). Cytokinesis failure generating tetraploids promotes tumorigenesis in p53-null cells. Nature 437, 1043–1047.

Fukumura D, Jain RK (2007). Tumor microenvironment abnormalities: causes, consequences, and strategies to normalize. J Cell Biochem 101, 937–949.

Ganem NJ, Godinho SA, Pellman D (2009). A mechanism linking extra centrosomes to chromosomal instability. Nature 460, 278–282.

Ganem NJ, Pellman D (2007). Limiting the proliferation of polyploid cells. Cell 131, 437–440.

Gascoigne KE, Taylor SS (2008). Cancer cells display profound intra- and interline variation following prolonged exposure to antimitotic drugs. Cancer Cell 14, 111–122.

Gentric G, Maillet V, Paradis V, Couton D, L'Hermitte A, Panasyuk G, Fromenty B, Celton-Morizur S, Desdouets C (2015). Oxidative stress promotes pathologic polyploidization in nonalcoholic fatty liver disease. J Clin Invest 125, 981–992.

Gerlinger M, Rowan AJ, Horswell S, Larkin J, Endesfelder D, Gronroos E, Martinez P, Matthews N, Stewart A, Tarpey P, *et al.* (2012). Intratumor heterogeneity and branched evolution revealed by multiregion sequencing. N Engl J Med 366, 883–892.

Giam M, Rancati G (2015). Aneuploidy and chromosomal instability in cancer: a jackpot to chaos. Cell Division 10, 3.

Guo Y, Kim C, Ahmad S, Zhang J, Mao Y (2012). CENP-E–dependent BubR1 autophosphorylation enhances chromosome alignment and the mitotic checkpoint. J Cell Biol 198, 205–217.

Hanahan D, Weinberg RA (2011). Hallmarks of cancer: the next generation. Cell 144, 646–674.

Hanks S, Coleman K, Summersgill B, Messahel B, Williamson D, Pritchard-Jones K, Strefford J, Swansbury J, Plaja A, Shipley J, Rahman N (2006). Comparative genomic hybridization and BUB1B mutation analyses in childhood cancers associated with mosaic variegated aneuploidy syndrome. Cancer Lett 239, 234–238.

Hendzel JM, Wei Y, Mancini AM, Van Hooser A, Ranalli T, Brinkley RB, Bazett-Jones PD, Allis DC (1997). Mitosis-specific phosphorylation of histone H3 initiates primarily within pericentromeric heterochromatin during G2 and spreads in an ordered fashion coincident with mitotic chromosome condensation. Chromosoma 106, 348–360.

Holland AJ, Cleveland DW (2009). Boveri revisited: chromosomal instability, aneuploidy and tumorigenesis. Nat Rev Mol Cell Biol 10, 478–487.

Huang H, Hittle J, Zappacosta F, Annan RS, Hershko A, Yen TJ (2008). Phosphorylation sites in BubR1 that regulate kinetochore attachment, tension, and mitotic exit. J Cell Biol 183, 667.

Hut HM, Kampinga HH, Sibon OC (2005). Hsp70 protects mitotic cells against heat-induced centrosome damage and division abnormalities. Mol Biol Cell 16, 3776–3785.

Jha S, Sharma PK, Malviya R (2016). Hyperthermia: role and risk factor for cancer treatment. Achiev Life Sci 10, 161–167.

Kops GJPL, Weaver BAA, Cleveland DW (2005). On the road to cancer: aneuploidy and the mitotic checkpoint. Nat Rev Cancer 5, 773.

Kuznetsova AY, Seget K, Moeller GK, de Pagter MS, de Roos JA, Durrbaum M, Kuffer C, Muller S, Zaman GJ, Kloosterman WP, Storchova Z (2015). Chromosomal instability, tolerance of mitotic errors and multidrug resistance are promoted by tetraploidization in human cells. Cell Cycle 14, 2810–2820.

Lee AJ, Endesfelder D, Rowan AJ, Walther A, Birkbak NJ, Futreal PA, Downward J, Szallasi Z, Tomlinson IP, Howell M, *et al.* (2011). Chromosomal instability confers intrinsic multidrug resistance. Cancer Res 71, 1858–1870.

Lu KV, Chang JP, Parachoniak CA, Pandika MM, Aghi MK, Meyronet D, Isachenko N, Fouse SD, Phillips JJ, Cheresh DA, *et al.* (2012). VEGF inhibits tumor cell invasion and mesenchymal transition through a MET/VEGFR2 complex. Cancer Cell 22, 21–35.

Machida K, Liu JC, McNamara G, Levine A, Duan L, Lai MM (2009). Hepatitis C virus causes uncoupling of mitotic checkpoint and chromosomal polyploidy through the Rb pathway. J Virol 83, 12590–12600.

Manning AL, Longworth MS, Dyson NJ (2010). Loss of pRB causes centromere dysfunction and chromosomal instability. Genes Dev 24, 1364–1376.

Mayer TU, Kapoor TM, Haggarty SJ, King RW, Schreiber SL, Mitchison TJ (1999). Small molecule inhibitor of mitotic spindle bipolarity identified in a phenotype-based screen. Science 286, 971–974.

Musacchio A (2015). The molecular biology of spindle assembly checkpoint signaling dynamics. Curr Biol 25, R1002–R1018.

Nicholson JM, Macedo JC, Mattingly AJ, Wangsa D, Camps J, Lima V, Gomes AM, Doria S, Ried T, Logarinho E, Cimini D (2015). Chromosome mis-segregation and cytokinesis failure in trisomic human cells. Elife 4, 05068.

Nowell PC (1976). The clonal evolution of tumor cell populations. Science 194, 23–28.

Paez-Ribes M, Allen E, Hudock J, Takeda T, Okuyama H, Vinals F, Inoue M, Bergers G, Hanahan D, Casanovas O (2009). Antiangiogenic therapy

elicits malignant progression of tumors to increased local invasion and distant metastasis. Cancer Cell 15, 220–231.
Potapova TA, Seidel CW, Box AC, Rancati G, Li R (2016). Transcriptome analysis of tetraploid cells identifies cyclin D2 as a facilitator of adaptation to genome doubling in the presence of p53. Mol Biol Cell 27, 3065–3084.
Raynaud-Messina B, Mazzolini L, Moisand A, Cirinesi AM, Wright M (2004). Elongation of centriolar microtubule triplets contributes to the formation of the mitotic spindle in gamma-tubulin-depleted cells. J Cell Sci 117, 5497–5507.
Reynolds TY, Rockwell S, Glazer PM (1996). Genetic instability induced by the tumor microenvironment. Cancer Res 56, 5754–5757.
Rieder CL, Maiato H (2004). Stuck in division or passing through: what happens when cells cannot satisfy the spindle assembly checkpoint. Dev Cell 7, 637–651.
Rivlin N, Brosh R, Oren M, Rotter V (2011). Mutations in the p53 tumor suppressor gene: important milestones at the various steps of tumorigenesis. Genes Cancer 2, 466–474.
Rutledge SD, Douglas TA, Nicholson JM, Vila-Casadesus M, Kantzler CL, Wangsa D, Barroso-Vilares M, Kale SD, Logarinho E, Cimini D (2016). Selective advantage of trisomic human cells cultured in non-standard conditions. Sci Rep 6, 22828.
Sackton KL, Dimova N, Zeng X, Tian W, Zhang M, Sackton TB, Meaders J, Pfaff KL, Sigoillot F, Yu H, *et al.* (2014). Synergistic blockade of mitotic exit by two chemical inhibitors of the APC/C. Nature 514, 646–649.
Seifert G, Budach V, Keilholz U, Wust P, Eggert A, Ghadjar P (2016). Regional hyperthermia combined with chemotherapy in paediatric, adolescent and young adult patients: current and future perspectives. Radiat Oncol 11, 65.
Sennino B, Ishiguro-Oonuma T, Wei Y, Naylor RM, Williamson CW, Bhagwandin V, Tabruyn SP, You W-K, Chapman HA, Christensen JG, *et al.* (2012). Suppression of tumor invasion and metastasis by concurrent inhibition of c-Met and VEGF signaling in pancreatic neuroendocrine tumors. Cancer Discov 2, 270–287.
Sheltzer JM, Blank HM, Pfau SJ, Tange Y, George BM, Humpton TJ, Brito IL, Hiraoka Y, Niwa O, Amon A (2011). Aneuploidy drives genomic instability in yeast. Science 333, 1026–1030.
Sheltzer JM, Ko JH, Replogle JM, Burgos NCH, Chung ES, Meehl CM, Sayles NM, Passerini V, Storchova Z, Amon A (2017). Single-chromosome gains commonly function as tumor suppressors. Cancer Cell 31, 240–255.
Silkworth WT, Nardi IK, Scholl LM, Cimini D (2009). Multipolar spindle pole coalescence is a major source of kinetochore mis-attachment and chromosome mis-segregation in cancer cells. PLoS One 4, e6564.
Sloss O, Topham C, Diez M, Taylor S (2016). Mcl-1 dynamics influence mitotic slippage and death in mitosis. Oncotarget 7, 5176–5192.
Solimini NL, Xu Q, Mermel CH, Liang AC, Schlabach MR, Luo J, Burrows AE, Anselmo AN, Bredemeyer AL, Li MZ, *et al.* (2012). Recurrent hemizygous deletions in cancers may optimize proliferative potential. Science 337, 104–109.
Sotillo R, Schvartzman JM, Socci ND, Benezra R (2010). Mad2-induced chromosome instability leads to lung tumour relapse after oncogene withdrawal. Nature 464, 436–440.
Stemmann O, Neidig A, Köcher T, Wilm M, Lechner J (2002). Hsp90 enables Ctf13p/Skp1p to nucleate the budding yeast kinetochore. Proc Natl Acad Sci USA 99, 8585.
Storchova Z, Pellman D (2004). From polyploidy to aneuploidy, genome instability and cancer. Nat Rev Mol Cell Biol 5, 45–54.
Swanton C, Nicke B, Schuett M, Eklund AC, Ng C, Li Q, Hardcastle T, Lee A, Roy R, East P, *et al.* (2009). Chromosomal instability determines taxane response. Proc Natl Acad Sci USA 106, 8671–8676.
Targa A, Rancati G (2018). Cancer: a CINful evolution. Curr Opin Cell Biol 52, 136–144.
Taylor SS, Hussein D, Wang Y, Elderkin S, Morrow CJ (2001). Kinetochore localisation and phosphorylation of the mitotic checkpoint components Bub1 and BubR1 are differentially regulated by spindle events in human cells. J Cell Sci 114, 4385.
Tsai YC, Weissman AM (2010). The unfolded protein response, degradation from the endoplasmic reticulum, and cancer. Genes Cancer 1, 764–778.
van der Zee J (2002). Heating the patient: a promising approach? Ann Oncol 13, 1173–1184.
van Harn T, Foijer F, van Vugt M, Banerjee R, Yang F, Oostra A, Joenje H, te Riele H (2010). Loss of Rb proteins causes genomic instability in the absence of mitogenic signaling. Genes Dev 24, 1377–1388.
Vasudev NS, Reynolds AR (2014). Anti-angiogenic therapy for cancer: current progress, unresolved questions and future directions. Angiogenesis 17, 471–494.
Velichko AK, Petrova NV, Kantidze OL, Razin SV (2012). Dual effect of heat shock on DNA replication and genome integrity. Mol Biol Cell 23, 3450–3460.
Vertii A, Zimmerman W, Ivshina M, Doxsey S (2015). Centrosome-intrinsic mechanisms modulate centrosome integrity during fever. Mol Biol Cell 26, 3451–3463.
Weaver BA, Bonday ZQ, Putkey FR, Kops GJ, Silk AD, Cleveland DW (2003). Centromere-associated protein-E is essential for the mammalian mitotic checkpoint to prevent aneuploidy due to single chromosome loss. J Cell Biol 162, 551–563.
Weaver BA, Cleveland DW (2006). Does aneuploidy cause cancer? Curr Opin Cell Biol 18, 658–667.
Wust P, Hildebrandt B, Sreenivasa G, Rau B, Gellermann J, Riess H, Felix R, Schlag PM (2002). Hyperthermia in combined treatment of cancer. Lancet Oncol 3, 487–497.
Zhu J, Pavelka N, Bradford WD, Rancati G, Li R (2012). Karyotypic determinants of chromosome instability in aneuploid budding yeast. PLoS Genet 8, e1002719.